Chapter 2
Performance Evaluation of Bone–Implant System During Implantation Process: Dynamic Modelling and Analysis

Rudi C. van Staden, Hong Guan, Newell W. Johnson, and Yew-Chaye Loo

Abstract Inappropriate choice of dental implant type in relation to the detailed structure of bone at the site, and inadequate surgical technique has led to 5 % failure of dental implants worldwide. By using the finite element method, three typical implant insertion scenarios are modelled and evaluated in this chapter. The scenarios are implant thread forming, cutting and the combination of forming and cutting. The bone–implant system is modelled using three-dimensional finite element technique which incorporates realistic material properties in simulating the cancellous and cortical bone. The bone–implant contact is defined using 'surface-to-surface' discretisation and the arbitrary Lagrangian–Eulerian adaptive meshing scheme. In current practice many implant companies recommend thread cutting for normal bone and forming for compact bone so that implant stability can be ensured. Based on the findings of the present study, the combination of forming and cutting may also be recommended for clinical practice because it best matches the specified ideal stress level resulting in positive bone stimulation with minimum resorption. Stress information obtained in these three implant insertion scenarios will advance the understanding of bone response at an early stage of the osseointegration process and primary stability.

Keywords Dental implant • Implant insertion • Bone–implant system • Finite element modelling technique • Stress analysis

R.C. van Staden
College of Engineering and Science, Structural Mechanics and Sustainable Materials Research Group, Victoria University, Melbourne, VIC, Australia

H. Guan (✉) • Y.-C. Loo
Griffith School of Engineering, Griffith University, Gold Coast, QLD, Australia
e-mail: h.guan@griffith.edu.au

N.W. Johnson
Menzies Health Institute Queensland, Griffith University, Gold Coast, QLD, Australia

Q. Li, Y.-W. Mai (eds.), *Biomaterials for Implants and Scaffolds*, Springer Series in Biomaterials Science and Engineering 8, DOI 10.1007/978-3-662-53574-5_2

2.1 Introduction

2.1.1 Background

Development of an ideal substitute for missing teeth has been a major aim of dentistry for millennia [1]. Mouths which have missing teeth are frequently restored by 'conventional' prostheses (partial or total), fabricated from plastic and/or metal alloys supported by the remaining teeth and/or the soft tissues. In many cases, however, removable prostheses will not be satisfactory, e.g. because of the lack of retention and/or psychological inability to accept such an appliance. In these cases, dental prostheses retained by an implant are an attractive alternative. A dental implant is a biocompatible 'fixture', usually screw-like and commonly made from titanium which is surgically placed into a jawbone to support a crown which forms an artificial tooth. Implants made of commercially available pure titanium have established a benchmark in osseointegration, against which no other materials can compare in a number of ways. Osseointegration is defined as the formation of bony interface which links bone to the implant surface [2].

The long-term benefits of dental implants include restored oral functions, improved appearance, comfort, speech clarity and self-esteem. With the implant, the patient can eat more conveniently, and the associated inconvenience of removable partial or full dentures does not exist. In addition, an implant is able to protect the remaining natural teeth, stop bone loss and restore facial skeletal structure. As far as the cost is concerned, implants have been shown to be comparable or even less expensive overall than conventional prostheses such as crown and bridge restorations [3]. Although the cost of an implant is generally higher than that of a crown or a bridge, the life time of an implant can be longer [4].

Worldwide implant statistics show a high success rate: in excess of 95 % retention over a 5-year period if the devices are correctly designed, manufactured and inserted [5–12]. Implants are expected to function for life, and this may well be possible in many cases, given that the retention rate at 15 years has been reported to be as high as 90 % if proper and professional care was taken by the practitioner and patient [13]. Despite all these advantages, only 10 % of Australian patients have received single or multiple dental implants [14]. This is mainly due to the initial high costs. However, it has been suggested [14] that another reason of low implant usage in Australia could be the lack of clinical skills [15] and knowledge of comparatively more complicated and less well-known implantation techniques. This is because the failure mechanisms consequential to the stress distribution characteristics in the jawbone during the implantation process itself, as well as the healing and maintenance phases, are poorly understood. Inaccurate implant manufacturer guidelines and inadequate surgical techniques also contribute to the 5 % failure of implants.

2.1.2 Implantation Procedure and Scenarios

Prior to commencement of implant placement, careful and detailed planning is required to identify the shape and dimensions of the bone to correctly orientate the implant. Periapical, panoramic and tomographic radiographs or computer tomography (CT) scans are often taken to assist in identifying these anatomical details and also to locate the nerve. The implantation process is initiated by making a small incision into the gingival tissue at the proposed implantation site. After the bone is made visible, a pilot hole is drilled into the cortical bone using a round bur. Drills of diameters 2.2, 3.0, 3.6 and 3.9 mm may be used successively, to create the implantation site in the cortical and cancellous bone, when inserting a single implant of diameter 4.5 mm [12]. Other operations, such as countersinking or screw tapping, may be a further stage before the implant is placed into the jawbone. The entire operation is performed under local anaesthesia, and a constant supply of physiological saline during the procedure reduces heat and flushes away blood and bone fragments.

The implant is finally inserted manually, using a ratchet or using a surgical micromotor mechanically. Manual insertion of the implant generally requires an increased torque with insertion depth as a result of the relatively low insertion velocity. On the other hand, mechanical insertion is performed at increased velocity, and thus the torque remains constant regardless of the insertion depth. Generally, 1 week after surgery, the implantation site is checked by the clinician for complete soft tissue healing around the healing abutment (one-stage implants) or over the implants (two-stage healing) [12]. The healing period for osseointegration varies and is dependent on criteria such as primary stability of implant at time of placement, bone quality, the use of any grafted bone or otherwise, overall patient health and the expected masticatory forces.

The bone strength and cortical thickness are generally the determining factors for the insertion drill sizes and finally the implant diameter. As such, three typical implant insertion scenarios are often adopted clinically. They are implant thread forming (scenario one, S1), thread cutting (scenario two, S2) or forming and cutting (scenario three, S3). If the bone cavity is 0.25 mm smaller in diameter than the implant, S1 takes place. Sennerby and Meredith [16] have shown that stability is reduced at sites of S1, thereby increasing the possibility of implant failure. For a bone cavity that is 0.6 mm smaller in diameter than the implant, S2 occurs. S2 is ideal in which the implant cuts a new thread pattern into the bone around a cavity of smaller diameter. In this case, optimum implant stability can be achieved through the entire length of the implant. In practice, S2 is often recommended by implant companies [12, 17, 18]. Note that if an implant is placed into a cavity created by a newly extracted tooth, the diameter of the cavity will vary. Generally, this cavity will be of a larger diameter at the top than the bottom. Therefore S3 takes place during insertion [12]. The amount of forming or cutting would ultimately contribute to the biological response of the bone and subsequently the outcome of the implantation procedure.

2.1.3 Finite Element Technique

While inserting the implant, elevated compressive stress can obstruct blood supply and damage the cells particularly for dense bone which in turn would affect osseointegration. On the other hand, inadequate stress cannot stimulate bone remodelling properly, thereby compromising implant stability. An optimal stress level and distribution must therefore be sought during and after implantation for the jawbone to remain strong and healthy.

There have been limited publications available on the response of bone cells to mechanical forces [19]. Limited data from animal studies suggest a large range of stress–strain values for the mandible [20]. Furthermore, bone densities and the local cell and tissue responses are also dependent on the general health and systematic responses of the patient. As such, the stress condition in the jawbone will change accordingly. The effects of such a phenomenon on bone resorption or healing has not been researched adequately, and the long-term effects of such stresses are still unclear.

The finite element method (FEM) is showing overwhelming capability and versatility in its application to dentistry [21–26]. The FEM has proven to be a reliable tool in analysing stress levels and distributions in biological bone tissues and in tissue-implant interacting structures. The primary difficulties in simulating the mechanical behaviour of dental implants are the complex finite element meshing process and the modelling of living human bone tissue and its response to applied mechanical forces. In an attempt to reduce the potential risks of clinical failure, research has been mainly directed towards finding the most biocompatible materials with which the dental implants are manufactured.

Despite the considerable research efforts on finite element analysis (FEA) of implant-mandible structure under a condition of full osseointegration, research into the modelling of the entire implantation process is non-existent. The purpose of this study is to model the insertion process in a dynamic manner, including further advancement on the bone–implant contact modelling. The major implantation scenarios to be considered are S1, S2 and S3. The aim of this study is to advance the work of van Staden et al. [27] on stepwise simulation of the implantation process. This will help provide an improved understanding of how various thread forming or cutting processes affect the outcome of implantation.

2.2 Dynamic Modelling

Summarised herein are the bone–implant geometry and material properties, modelling details and contact simulation for simulating the implantation process. The dynamic modelling of the implantation process requires the definition of complex bone–implant contact behaviour and material properties.

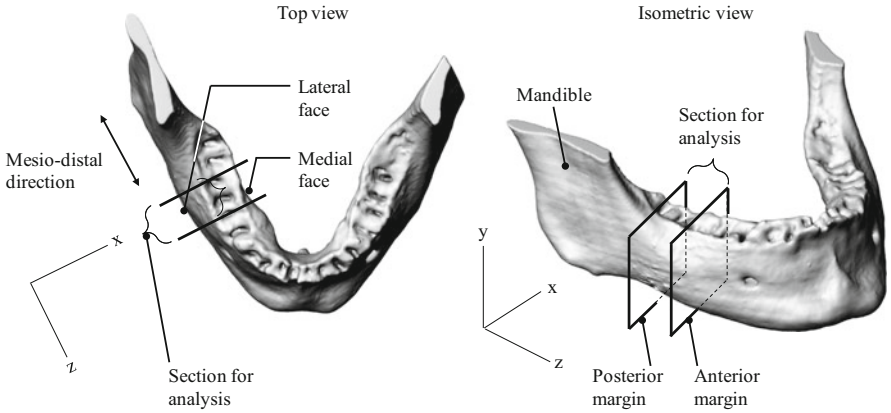

Fig. 2.1 Location of three-dimensional slice in a mandible

2.2.1 *Bone–Implant System Geometry and Material Properties*

All the modelling and analyses are carried out using ABAQUS in this study [28]. Data acquisition for bone dimensions are based on computed tomography (CT) scanned images. From these images, a section from the human mandible is taken as illustrated in Fig. 2.1. The bone is categorised as 'soft quality' or type IV bone.

The geometry of the sectioned bone structure for analysis, as identified in Fig. 2.1, has been smoothed out with geometrical discontinuities removed. This model is illustrated in Fig. 2.2 with different dimensions of bone cavities. S1, S2 and S3 take place, respectively, for bone cavity diameters of 4.25, 3.9 mm and the combination of these two. Note that for S3 the bone cavity has a 1.5° taperage due to the difference in the top (4.25 mm) and bottom (3.9 mm) diameters of the cavity, as shown in Fig. 2.2 (b). A conical implant is considered herein with 2° of taper angle, a helical thread and three primary cutting faces. A typical implant of 4.5 mm in diameter and 11 mm in length is presented in Fig. 2.3.

Realistic material behaviour of the cancellous bone requires the definition of elastic and plastic properties. Plastic behaviour is defined because it is expected that the bone would exceed its maximum yield stress during implantation. Note that the stress–strain relationship for the bone is defined up to the point of fracture (see Fig. 2.4), as obtained by Burstein et al. [29] from human femur and tibia specimens. The detailed material properties of the bone adopted in this study are listed in Table 2.1. The friction coefficient between the surfaces of bone and commercially available pure titanium was obtained from Choubey et al.'s [30] fretting wear tests performed in a salt solution. Young's modulus, Poisson's ratio and density of the implant are, respectively, 102GPa, 0.3 and 4.54×10^{-6} kg/mm^3.

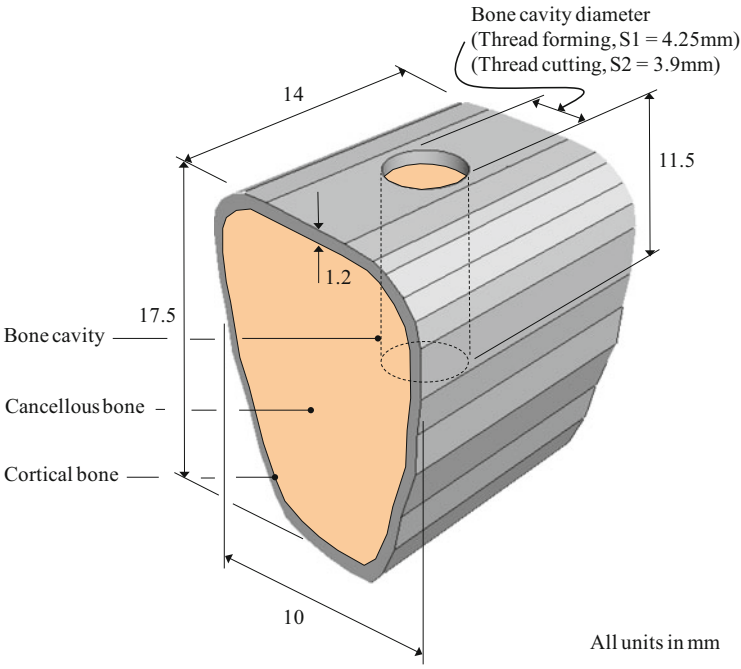

a) Thread forming, S1 or cutting, S2

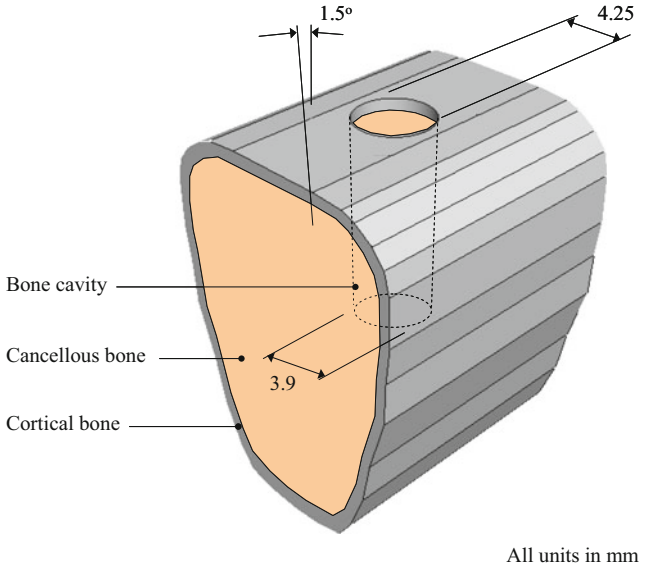

b) Thread forming and cutting, S3

Fig. 2.2 Details of mandibular bone and cavity

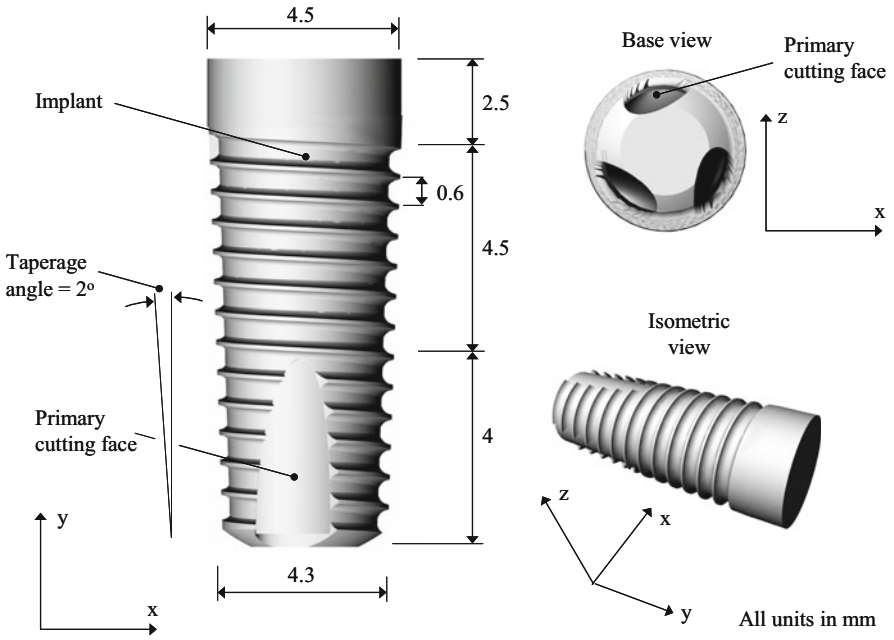

Fig. 2.3 Details of a typical implant design

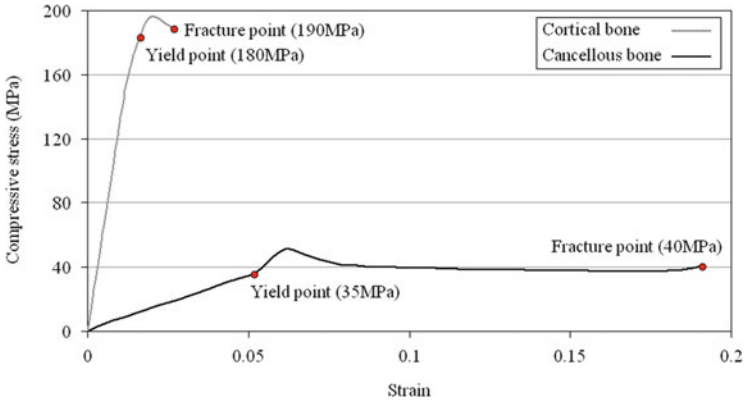

Fig. 2.4 Stress–strain behaviour [29]

2.2.2 Modelling Details

During implantation, the implant can be inserted manually or mechanically. A manual insertion process was modelled previously [27] in a stepwise manner with a torque applied to the implant that increases with time. The present study

Table 2.1 Material properties of cancellous and cortical bone

		Cancellous bone	Cortical bone	Sources	Specimen details
	Young's modulus, E ($\times 10^3$ N/mm^2)	0.7	9	[29]	Human femur and tibia (type IV)
Elastic	Poisson's ratio, v	0.35	0.3		
	Density, ρ ($\times 10^{-7}$ kg/mm^3)	5.3	18		
Plastic	Yield stress (N/mm^2)	35	180	(Fig. 2.4)	
	Plastic strain	0.135	0.015		
Contact	Friction coefficient	0.61		[30]	Human femur

deals with mechanical insertion whereby the process of implantation is continuous with a constant torque.

Figure 2.5 illustrates a constant torque of 450 Nmm with an insertion velocity of 0.31 mm/s applied to the top of the implant. The velocity is based on an insertion depth of 11 mm over a total period of 36 s. Note that the bone cavity is 11.5 mm in depth, thereby leaving 0.5 mm between the bottom of the implant and bone to store blood and bone fragments. Shown in Fig. 2.5 are the fixed constraints on the bone surfaces (anterior and posterior) along the mesiodistal direction of such a hypothetical human mandible.

The finite element models of the bone and implant are meshed automatically within the program by using tetrahedral elements. As an example, for the bone and implant models of S2, the total numbers of elements and nodes are 85,234 and 67,567, respectively. The elements on the entire cavity surface are refined to 40 % of the average mesh size on the anterior and posterior faces. This would enable to obtain more accurate results during implant insertion. Mesh convergence was undertaken on the similar models in our previous work [31].

2.2.3 Contact Simulation

Interaction between the bone and implant during dynamic simulation of the implantation process is complex and requires proper definition of contact conditions. In the present study, the contact is defined in ABAQUS [28] using 'surface-to-surface' discretisation because it provides more accurate stress and pressure results than node-to-surface discretisation. Surface-to-surface contact is incorporated in the modelling by using the constraint enforcement methods where the surfaces do not require matching meshes (i.e. node-to-node contact). This is because ABAQUS [28] enforces conditional constraints on each surface to simulate contact conditions. In addition, the contact interaction properties are also required to be defined for the contact pair.

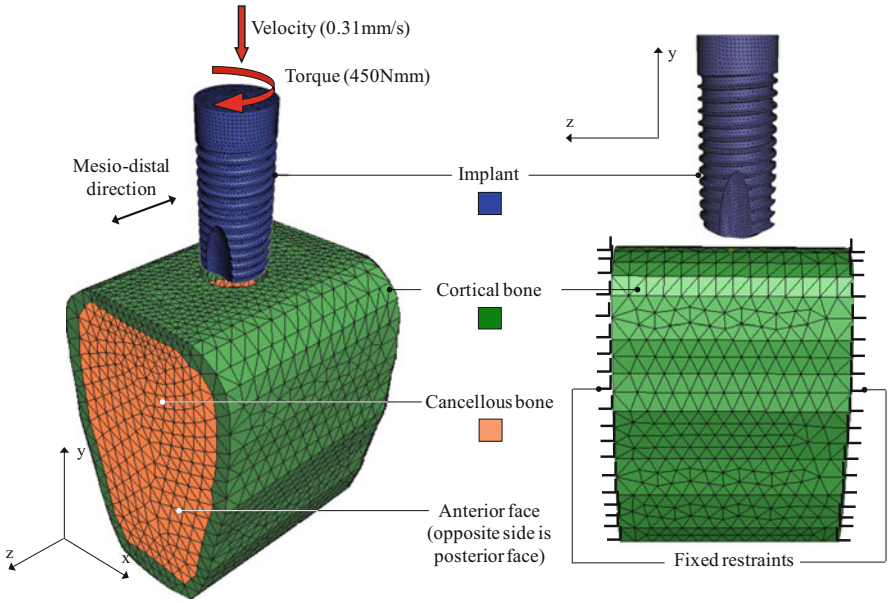

Fig. 2.5 Loading and restraint conditions applied to the bone and implant

As illustrated in Fig. 2.6, the definition of the two contact surfaces is achieved by setting the side and bottom surfaces of the implant as the master surface. The slave surface includes the entire inner surface of the bone cavity and the top ring area of 0.5 mm width on the cortical surface. This top ring area defines the contact between the implant and the top of cortical bone because the implant diameter is larger than the cavity. In accordance with the surface-to-surface definition, contact constraints are enforced in an average sense over the slave surface, rather than at discrete points, such as at slave nodes in the case of node-to-surface discretisation. Therefore, penetration of individual master nodes into the slave surface is allowed; however, the reverse is not permitted.

Defining the contact is yet to be completed because under large deformation, ABAQUS [28] defaults the slave surface to be penetrated by the master nodes, as illustrated in Fig. 2.7 (a). As such, the material properties of the slave surface cannot be properly defined after deformation. Therefore, adaptive meshing technique must be employed so that the material moves with the slave surface mesh at all times during the insertion simulation.

The adaptive meshing scheme specified in ABAQUS [28] is termed 'arbitrary Lagrangian–Eulerian' (ALE) because it combines the Lagrangian and Eulerian methods. The Lagrangian method is used to track the path of the element so that no nodal penetrations occur. However, this method alone still allows material to move independently of the mesh. The Eulerian method, on the other hand, takes into account conservation of mass so that the material is conserved within the elements. The ALE combines these two methods so that if nodal penetrations occur,

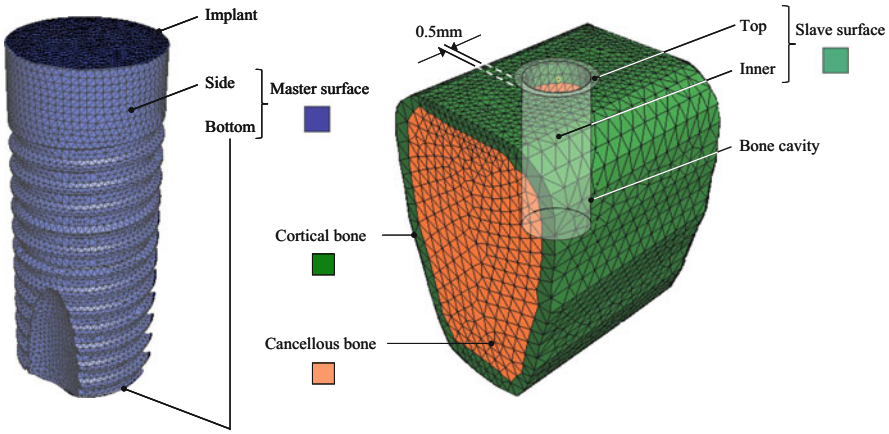

Fig. 2.6 Master and slave surfaces

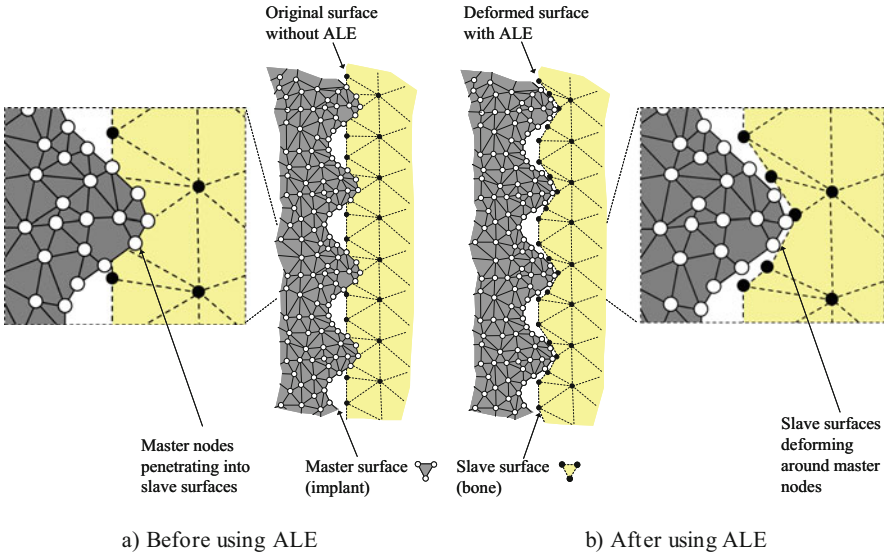

Fig. 2.7 Adaptive meshing

forces that are a function of the penetration distance are applied to the master nodes to counteract the penetration, with equal and opposite forces acting on the slave surface at the penetration points. Detailed in Fig. 2.7 (b) is an example of the slave surface deforming around the master nodes after ALE is applied.

The next step in defining a surface-based contact is to model the contact interaction properties. In this study, the tangential properties of the surface are defined using friction coefficient (see Table 2.1) and the normal properties defined as hard contact. Hard contact is implemented to ensure that the master nodes are in

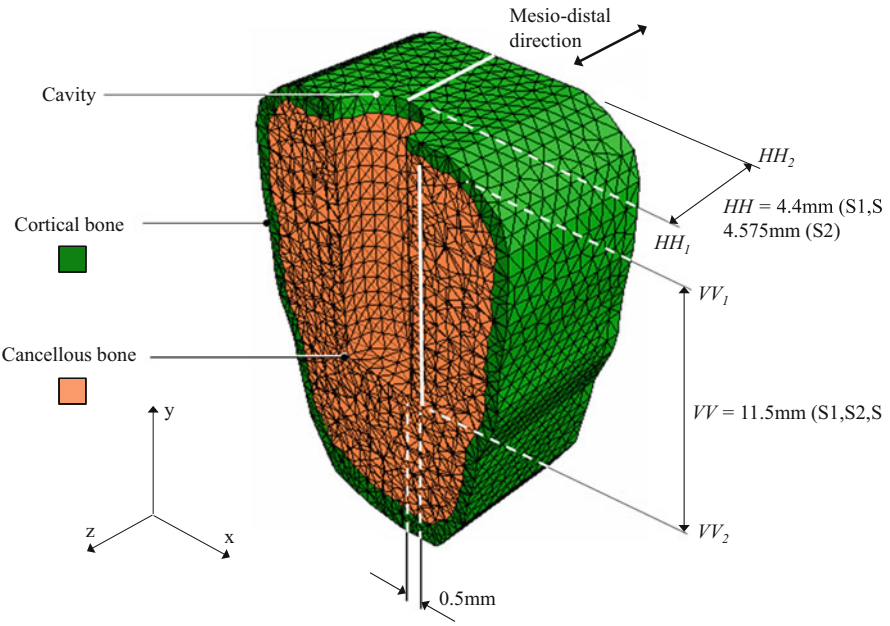

Fig. 2.8 Stress measurement within cancellous and cortical bone

complete contact with the slave surface therefore not allowing transfer of any tensile stresses across the interface.

2.2.4 Criteria for Stress Measurements

The stress within the bone are considered to be the determining factor for understanding both bone fracturing during insertion and subsequent bone resorption. The von Mises stresses are measured along the lines *VV* in the cancellous bone and *HH* in the cortical bone, as shown in Fig. 2.8. Line *VV* is 11.5 mm in length for all bone cavity diameters; however, the length of *HH* is dependent on the bone cavity dimensions. The length of line *HH* is 4.4 mm for S1 and S3 and 4.6 mm for S2. Due to the irregularity of the mesh, a straight line of nodes at which the stress is measured is only approximated for both *VV* and *HH*. The distance of *VV* away from the bone cavity surface is fixed at 0.5 mm. The stress measurement line, *HH*, is positioned to capture the most severe stress levels. The beginning and end points of *VV* (i.e. V_1 and V_2) and *HH* (i.e. H_1 and H_2) are also identified in Fig. 2.8 for ease of discussion.

2.3 Results and Discussion

The following subsections detail the von Mises stresses in both cancellous and cortical bone, each with discussions for the three insertion scenarios (S1, S2 and S3). The stresses are measured along the lines *VV* and *HH* during the entire insertion process. Sections 2.3.1 and 2.3.2 present the stress characteristics within the cancellous and cortical bone, respectively, for S1, S2 and S3. The stress profile within the cancellous and cortical bone for the selected stages of insertion is presented followed by stress contour plots in subsequent figures illustrating the stress characteristics. It is assumed that the implant tip is pushed slightly into the top surface of cortical bone prior to the application of the torque. This corresponds to 1.8 s or 0.5 mm insertion depth where the stresses are measured from the stress profiles shown in Figs. 2.9, 2.10, 2.12, 2.13, 2.14 and 2.15 (a). For ease of discussion, stress profiles produced for 3.6–36 s at 10.8 s time steps (Figs. 2.9, 2.10, 2.12, 2.13, 2.14 and 2.15 (b), (c), (d), (e) and (f)) are detailed in Sections 2.3.1 and 2.3.2.

2.3.1 Cancellous Bone

2.3.1.1 Thread Forming, S1

For most of the time steps, it is evident that when the insertion depth increases, the stress level also increases. This is because the surface area of contact between the bone and implant increases, and therefore a larger amount of the applied torque is transferred to the bone.

As seen in Fig. 2.9 (a) and (b), when the implant is inserted 0.5 mm into the cortical bone, the stress level within the cancellous bone is relatively low (0.07 MPa) because the implant and cancellous bone are not yet in direct contact. At this stage, the only stresses experienced in the cancellous bone are those transferred from the cortical bone. Figure 2.9 (c) also indicates that for an insertion depth of 1.1 mm, the global stress peak occurs at VV_1. This peak is caused by the primary cutting faces together with the stresses transferred from the cortical bone.

At a depth of 4.4 mm, the cancellous bone experiences an increase in the stress further away from VV_1 because the implant is inserted deeper into the bone (Fig. 2.9 (d)). At 7.7 mm depth, the stress increases slightly compared to the previous stages (i.e. average from 0.93 to 1.24 MPa). The stress contour distributes more evenly throughout the bone adjacent to the implant as the insertion depth increases, as illustrated in Fig. 2.9 (e).

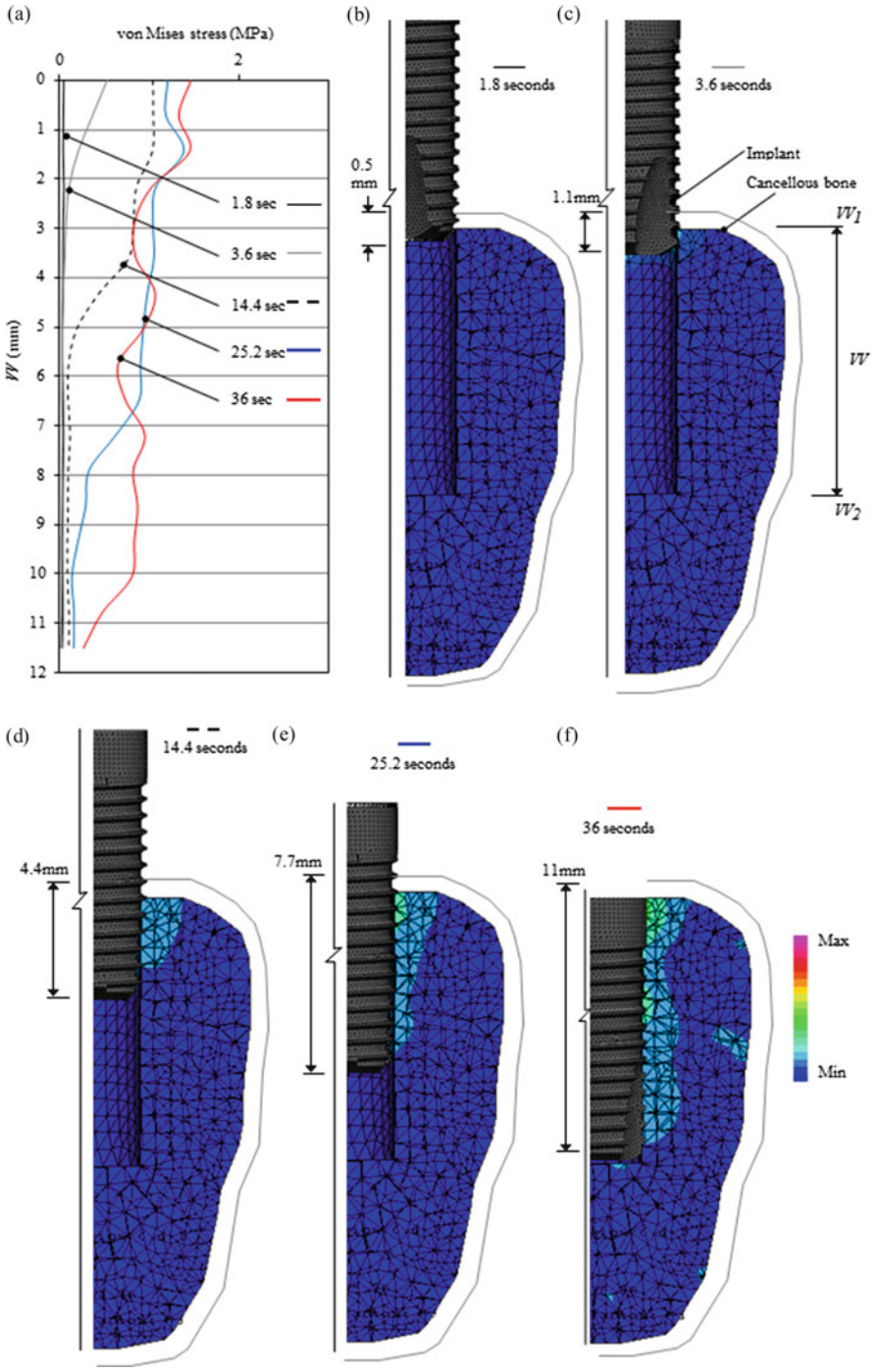

Fig. 2.9 Stress characteristics in cancellous bone at five insertion stages during thread forming

At the final stages of insertion (Fig. 2.9 (f)), the stress at 11 mm insertion depths increase (1.48 MPa) compared to all the previous stages. The global stress peak for this insertion step is a result of the abrupt change in implant geometry where the implant neck establishes contact with the cancellous bone.

2.3.1.2 Thread Cutting, S2

Similar to S1, S2 also causes increased stresses when the insertion depth increases. From the time periods 1.8 and 3.6 s, the stresses (0.3 and 1.2 MPa) are significantly higher than those found during S1 (0.07 and 0.51 MPa, correspondingly), as illustrated in Fig. 2.10. This is because the diameter of the bone cavity is reduced in S2. This also results in a larger stressed region towards the outer edge of the cortical bone, as evident in the stress contour plots (Fig. 2.10 (b), (c), (d), (e) and (f)). It is also found that stress peaks occur at the same locations as found for S1.

At 14.4 s, as detailed in Fig. 2.10 (d), the increased stresses move further down and away from VV_1 due to the increased insertion depth. The stress contours show to be more unevenly distributed when compared to the previous stages. The stress peak at VV_1 is much higher (4.0 MPa) than that found in S1.

At the final insertion stages, the stress profile and contour are shown to be more evenly distributed as compared to the corresponding ones in S1. The stress peak occurs at 4.7 mm (5.34 MPa) from VV_1 for the insertion depth of 11 mm. Similar to S1, this stress peak is again a result of the implant neck commencing contact with the cancellous bone.

Figure 2.11 illustrates, as an example, the progressive stress contours within the cancellous bone during the entire implantation process for the thread cutting scenario (S2). The corresponding time, insertion depth and implant revolutions are also indicated in the figure. Note that only the exterior surface of the implant is shown for ease of viewing the stress contours within the bone.

2.3.1.3 Thread Forming and Cutting, S3

Similar to S1 and S2, when the insertion depth increases, the stresses within the cancellous bone also increase for S3. From 1.8 to 3.6 s, as presented in Fig. 2.12 (a), the stress levels (0.09 and 0.4 MPa) are similar to those of S1 (0.07 and 0.5 MPa) but smaller than those for S2 (0.3 and 1.2 MPa). This is due to the geometrical changes of the bone cavity. The stress contours are also more comparable to those of S1, as detailed in Fig. 2.12 (b) and (c).

At 14.4 s, as illustrated in Fig. 2.12 (d), the stress level (1.3 MPa) is slightly higher than that of S1 (1.0 MPa) but significantly lower than S2 (4.0 MPa). A global stress peak at 14.4 s occurs along the line VV because of the geometry of the primary cutting faces and the reduced diameter of the bone cavity which induce a slight change in the stress contour when compared to S1.

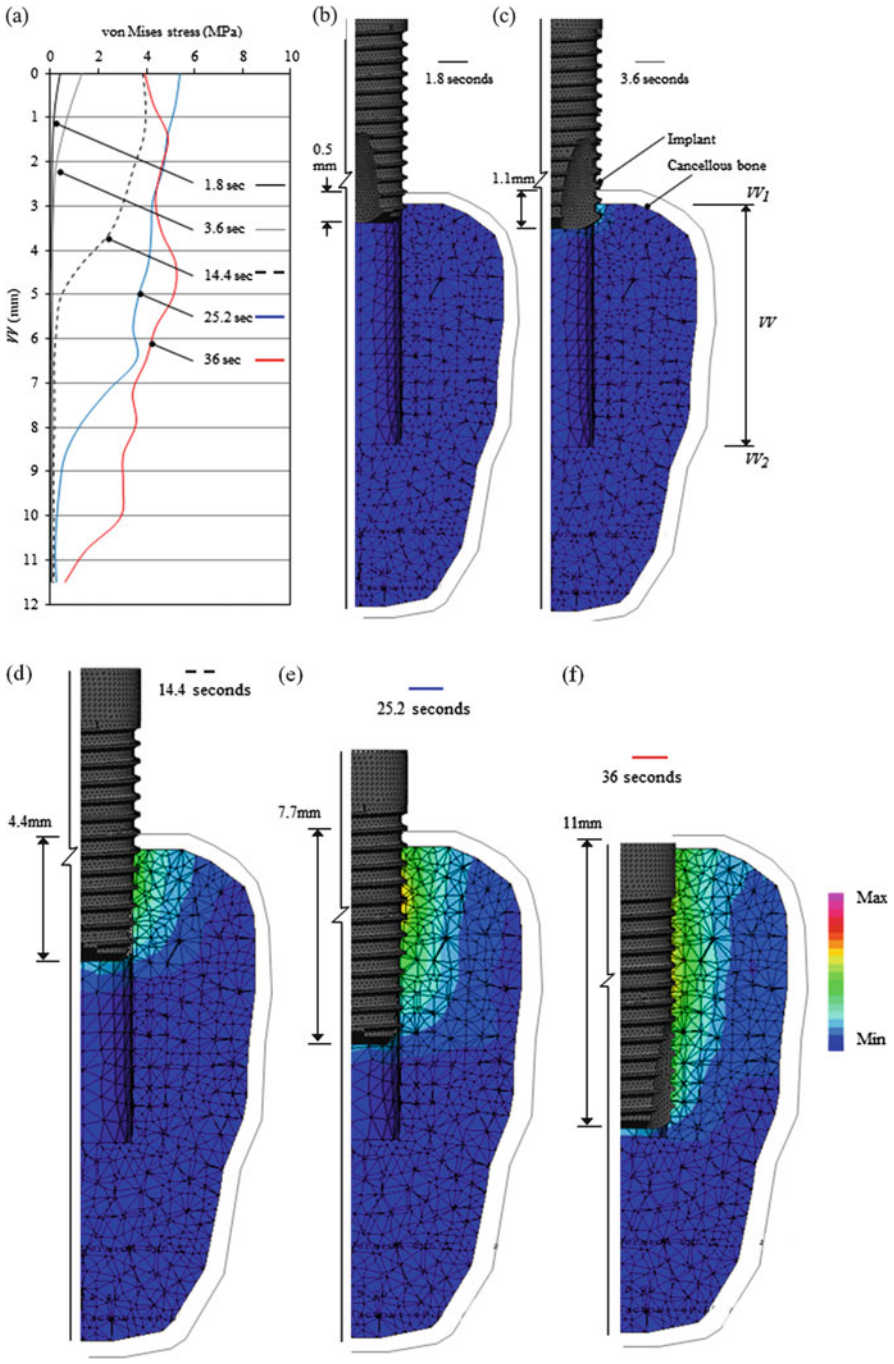

Fig. 2.10 Stress characteristics in cancellous bone at five insertion stages during thread cutting

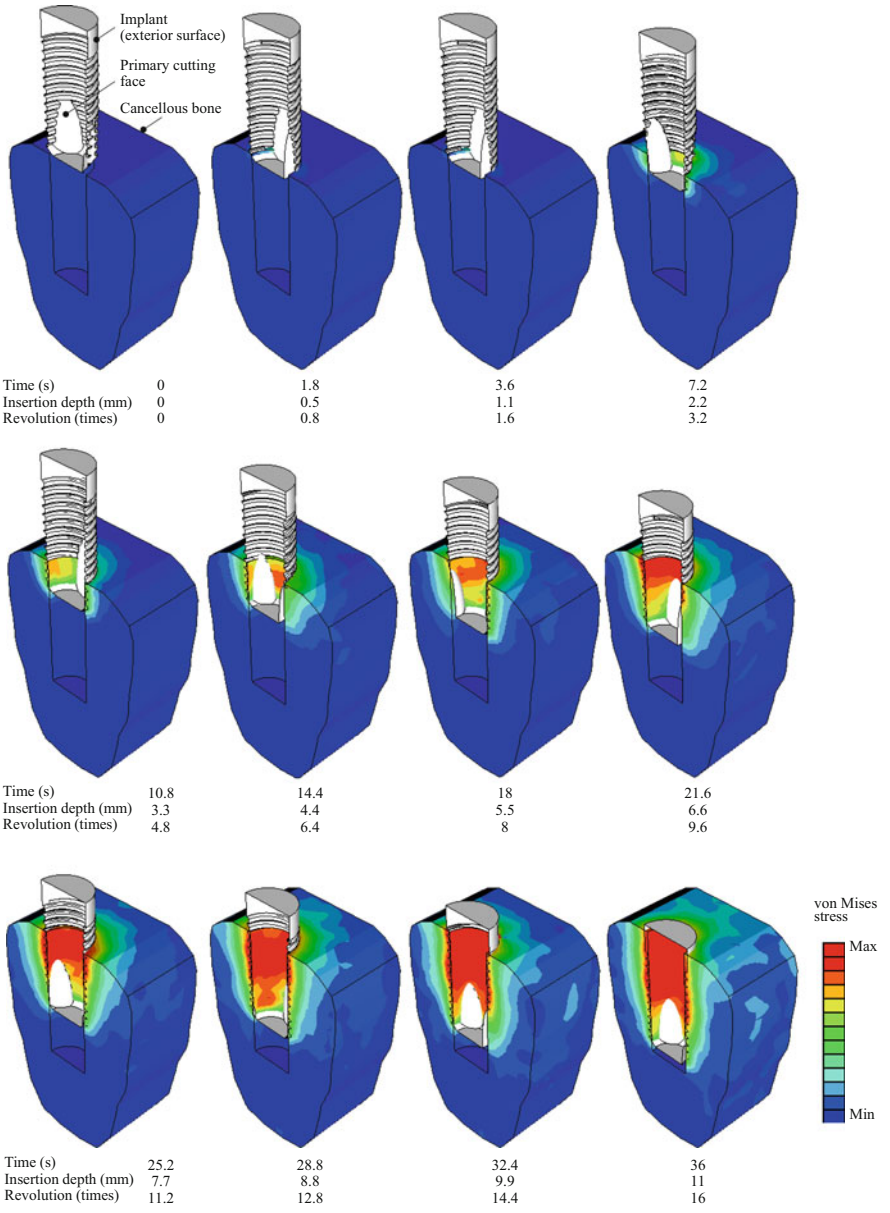

Fig. 2.11 Progressive stress contours in cancellous bone during the entire implantation process (thread cutting, S2)

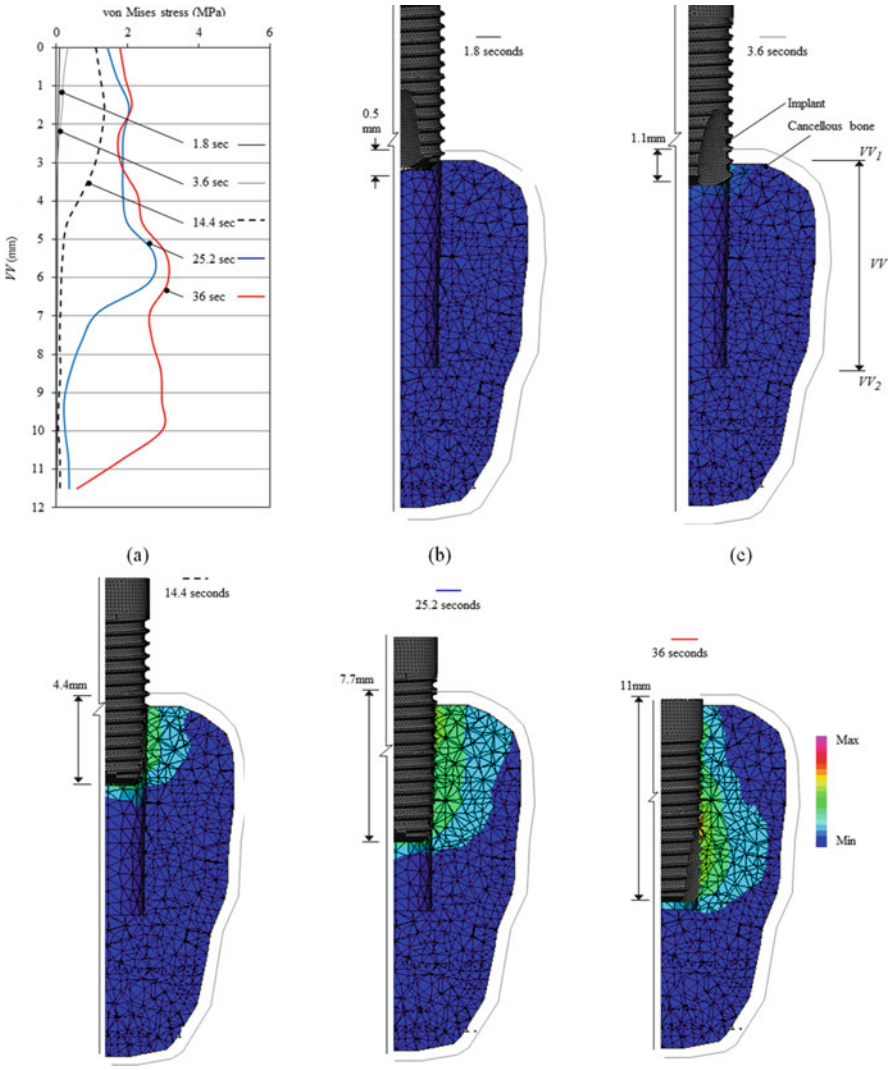

Fig. 2.12 Stress characteristics in cancellous bone at five insertion stages during thread forming and cutting

The stress characteristics at 25.2 s show an increase in magnitude (2.7 MPa) when compared to that of S1 (1.4 MPa) and a decrease as compared to S2 (5.2 MPa). The stress profile shown in Fig. 2.12 (a) indicates that a stress peak occurs at a region close to the primary cutting faces. A reduction in bone cavity diameter gives a stress contour that is more comparable to that of S1 than S2.

At 11 mm insertion depth, the stress shows a significant increase; however, the stress at VV_1 remains comparable to that found for S1. The increase in stress is a result of the reduced cavity diameter. Note also that the stress contour is more comparable to S2.

2.3.2 Cortical Bone

2.3.2.1 Thread Forming, S1

In general, the stress within the cortical bone decreases from HH_1 towards HH_2 for all insertion steps. The stress profiles presented in Fig. 2.13 (a), shows a significant stress increase at point HH_1 from 1.6 MPa (1.8 s, before the primary cutting faces are in contact) to 9.2 MPa (3.6 s, when contact is established). Such a large variation in stress is particularly evident in the contour plots (Figs. 2.13 (b) and (c)).

For 14.4 s, the stress next to the implant increases to 14.4 MPa. Such an increase is due to the increased cortical bone to implant contact as a result of the narrowing gaps between the cutting faces as the insertion step increases.

At 25.2 s, the stress contour only exhibits a marginal increase in stress (i.e. 16.4 MPa) because the cutting faces are no longer in contact with the cortical bone at HH_1. For the 36 s, an increase in stress (i.e. 20.4 MPa) is found when compared to 25.2 s because the implant neck is in contact with the cortical bone at this stage.

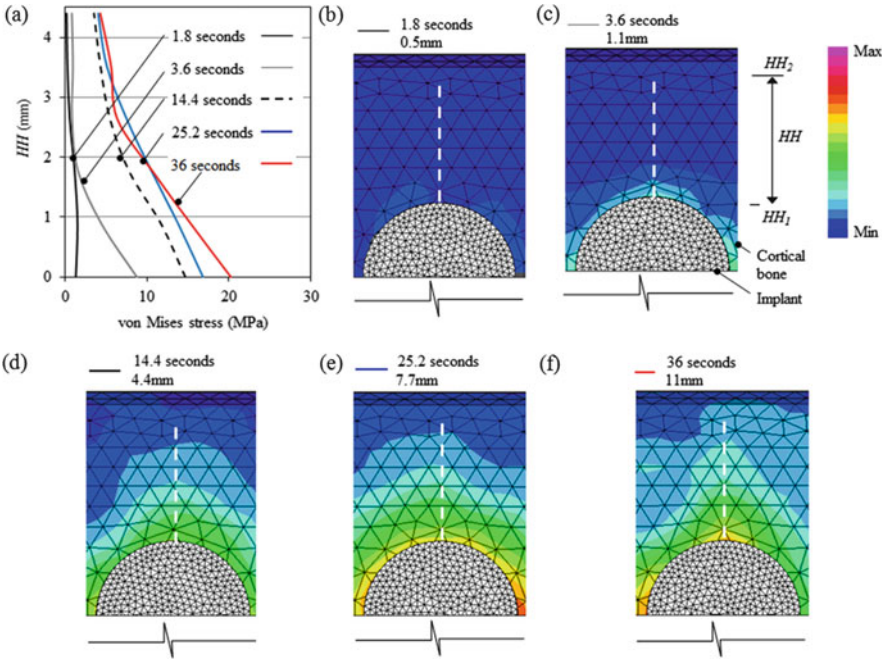

Fig. 2.13 Stress characteristics in cortical bone at five insertion stages during thread forming

2.3.2.2 Thread Cutting, S2

Similar stress characteristics are found for S2 as with S1. However, S2 induces significantly higher stresses within the cortical bone, with a maximum of 11.4 MPa compared to 9.2 MPa at 3.6 s, as illustrated in Fig. 2.14 (a). At an insertion depth of 4.4 mm, a maximum stress of 20.1 MPa occurs at the implant neck, which is significantly higher than that found at the same insertion step during S1 (14.4 MPa). The stress contours shown in Figs. 2.14 (b) to (f) also confirm such an increase in stresses.

2.3.2.3 Thread Forming and Cutting, S3

The stress characteristics are again comparable to those found for S1 or S2, as detailed in Fig. 2.15. In general, the stress characteristics are between those of S1 and S2, but closer to the S1 scenario. This is because the stresses are only measured at the top of the bone cavity where its diameter is identical to that of forming (i.e. S1).

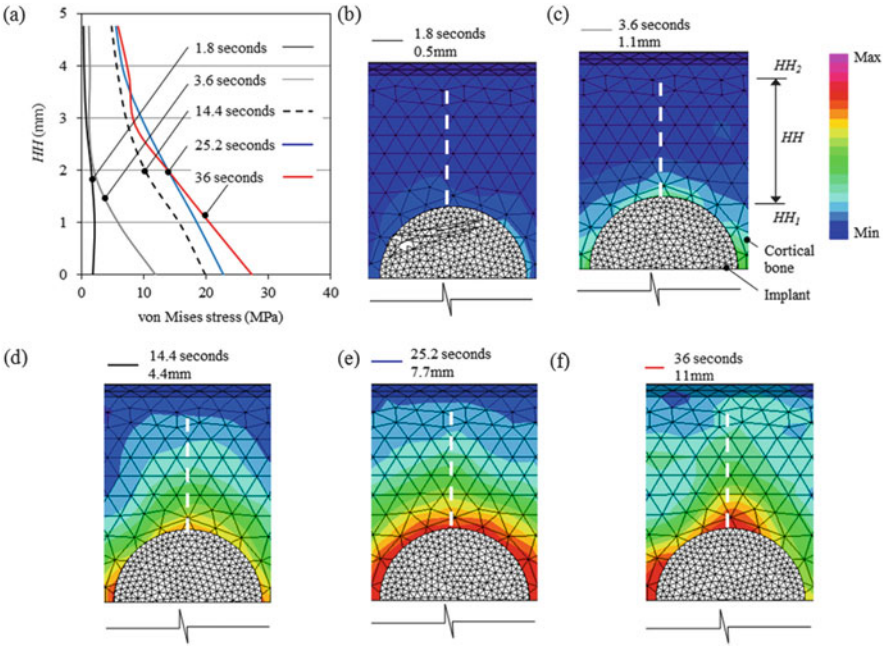

Fig. 2.14 Stress characteristics in cortical bone for five insertion stages during thread cutting

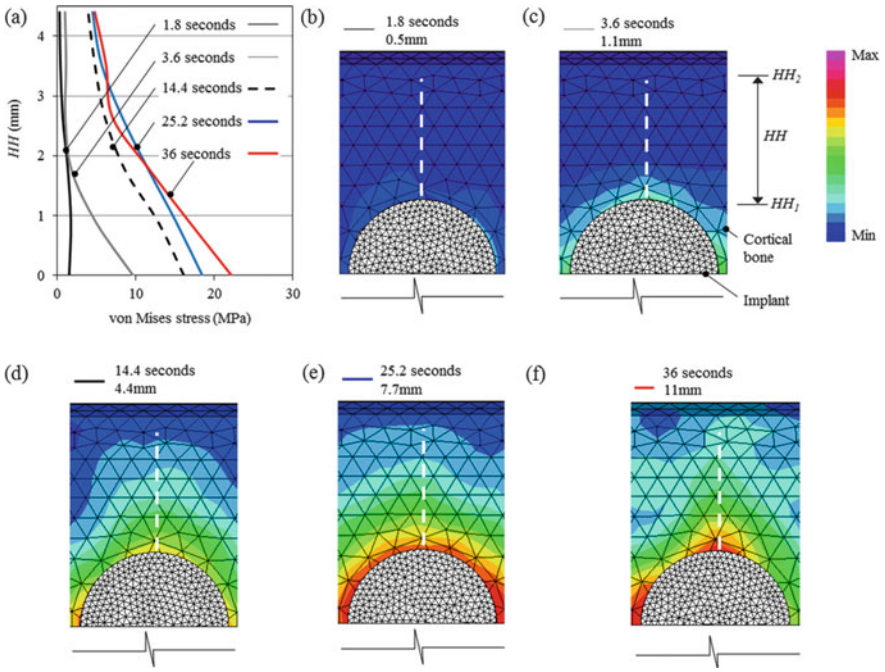

Fig. 2.15 Stress characteristics in cortical bone for five insertion stages during thread forming and cutting

2.3.3 Maximum Stresses in Different Implantation Scenarios

This subsection summarises the maximum von Mises stresses for 11 selected insertion depths of the S1, S2 and S3 scenarios. Based on the data shown in Figs. 2.9, 2.10, 2.11, 2.12, 2.13, 2.14 and 2.15, the maximum stresses along lines *VV* and *HH* are summarised in Table 2.2. As the insertion depth increases, the maximum stress along the line *VV* takes place at varied distances, *dv* away from VV_1. However for cortical bone, the maximum stresses always occur at HH_1.

Table 2.2 reveals that for the cancellous bone, the maximum stresses for S3 are closer in magnitude to those of S1 at initial insertion depths. This is because the upper bone cavity diameters are similar to each other for these two case scenarios. As the insertion depth increases, the maximum stress of the combined scenario (S3) approaches a magnitude which is approximately halfway between the S1 and S2 scenarios. This is due to the reduction in bone cavity diameter in the lower region which is approaching to that of the S2 scenario. In the initial insertion depths in general, the maximum stresses along the line *VV* occur on or close to VV_1. However, for the insertion depths 8.8–11 mm, the maximum stresses occur further away from VV_1 due to the decrease in the bone cavity diameter. For the cortical bone, the maximum stresses at HH_1 for S3 are in between those of S1 and S2 from 0.5 to 2.2 mm insertion depths. For the insertion depths from 3.3 to 11 mm, the

Table 2.2 Maximum von Mises stresses (MPa) along line *VV* and at point HH_1

	Forming, S1			Cutting, S2			Forming and cutting, S3		
Insertion depth (mm)	*VV*	*dv*	HH_1	*VV*	*dv*	HH_1	*VV*	*dv*	HH_1
0.5	0.07	0.0	1.6	0.3	0.0	2.1	0.09	0.0	2.06
1.1	0.51	0.0	9.2	1.2	0.0	11.44	0.44	0.0	9.8
2.2	0.96	0.7	9.9	3.92	0.71	12.1	0.99	0.82	10.9
3.3	0.8	0.0	14.37	2.5	0.0	20.3	1.09	1.48	16.1
4.4	1.08	0	14.4	4.02	0.79	20.1	1.34	1.66	16.14
5.5	0.9	1.47	23.4	4.8	0	32	1.11	0.87	26.3
6.6	1.09	0	22.1	4.57	0.97	30.2	1.48	1.59	24.7
7.7	1.46	1.41	16.4	5.2	0	22.6	2.76	5.6	18.4
8.8	1.18	1.65	20.7	5.24	2.75	28.5	2.21	3.91	22.9
9.9	1.94	3.62	17.2	5.1	4.07	22.8	2.32	7.52	19
11	1.48	1.47	20.4	5.34	4.61	28.1	3.02	9.77	22.2

dv in mm

stress levels of S3 are closer in magnitude to S1 than S2, because the cavity diameters at the top of the cortical bone are the same for S2 and S3.

2.3.4 Clinical Significance

The optimal or desirable stress levels to be experienced by local bone during implantation have not yet been firmly established. However, according to Rieger et al. [32] and O'Mahony et al. [33], the desirable stress level lies between 1.72 and 2.76 MPa. The material structure of the cancellous bone makes it more sensitive to fracture than the cortical bone. The minimum and maximum stress profiles along the line *VV* produced by S1, S2 and S3 are plotted in Fig. 2.16 together with an ideal stress range (presented by the lower and upper limits) for cancellous bone growth and repair. Note that the minimum stress profiles are obtained at 1.8 s and the maximum at 36 s. On the basis of present knowledge, if the stress falls below 1.72 MPa, bone may not be stimulated adequately for effective healing and osseointegration. On the other hand, if the stress exceeds 2.76 MPa, bone resorption may occur, which contributes to loosening and potential failure of the implant. The ideal bone response will be achieved when the stress remains between these limits.

For all three insertion scenarios, the minimum stress profiles at 1.8 s are considerably below the lower limit of the stimulation stress (i.e. 1.72 MPa). For S1 (forming), the maximum stress profile (at 36 s) still does not reach the lower stress limit of 1.72 MPa. The low stress level produced by S1 may adversely affect initial retention of the implant which confirms the findings of Sennerby and Meredith [16] in that thread forming reduces implant stability. For S2 (cutting), the maximum stress profile at 36 s shows that bone resorption may occur around the implant because the upper stress limit of 2.76 MPa is exceeded for most of the

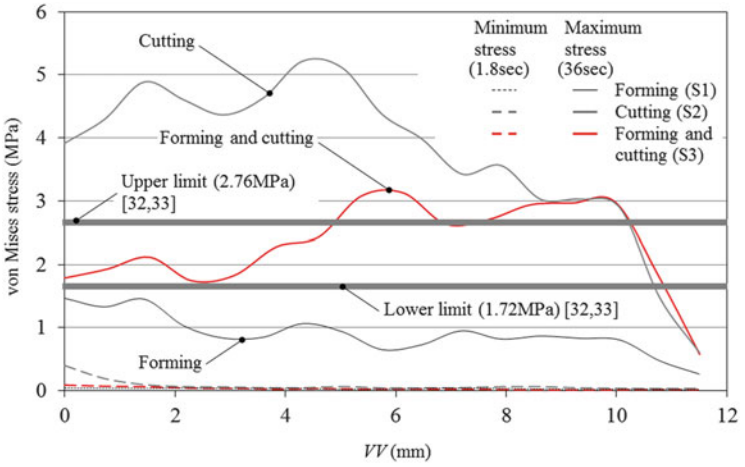

Fig. 2.16 Maximum and minimum stress profiles during implantation

locations along line *VV*. Overall, S3 (forming and cutting) best satisfies the ideal level of stress suggested in the literature. In current practice, many implant companies [12, 17, 18] generally recommend S2 for normal bone (i.e. type III or IV [34]) and S1 for compact bone (i.e. type I or IV) so that implant stability can be compromised. Based on the findings of this study, S3 may also be recommended for clinical practice.

It is important to note, however, that these findings have not modelled the fracture of bone through element deletion nor the effects of blood flow which influences contact friction. Incorporating such aspects into the finite element analysis merits further investigation.

2.4 Conclusion

2.4.1 Research Outcomes

The von Mises stress characteristics within the cancellous and cortical bone are evaluated for thread forming (scenario one, S1), cutting (scenario two, S2) and combined forming and cutting (scenario three, S3). With the adaptive meshing and contact interaction properties available in ABAQUS [28], realistic stress characteristics are modelled. The continuous dynamic simulation and implant cutting faces prove to be the major factors that distinguish the present results from those achieved in the stepwise simulation [14].

For S1, the stress levels within the cancellous and cortical bone are less than those in S2 and S3 because of the reduced bone to implant surface contact area. However, the stresses within the cancellous bone are only slightly reduced for S3

during the initial insertion steps. Then at later insertion steps, the stress within the cancellous bone (at any location along the line *VV*) increases to be at a level approximately halfway between those of S1 and S2. For cortical bone, the magnitude increases less significantly as the implant insertion depth progresses. The minor variation is due to the geometrical differences of the bone cavity. In both cancellous and cortical bone, the primary cutting faces induce stress peaks during the initial insertion stages (0.55–2.2 mm). This is because of the abrupt changes in geometry of the cutting faces. For the final insertion stages (9.9 and 11 mm) the change in implant section (i.e. implant neck establishes a contact with the cancellous bone) results in stress peaks within the cancellous bone.

The innovation of this research lies in the increased understanding of the stress characteristics in bone during the implantation process. This is likely to advance biomechanics of implantation surgery appreciably. Mechanical loosening after implantation is a significant challenge for most endoprosthetic procedures, and this research presents useful insights.

2.4.2 Recommendations for Further Developments

Optimisation techniques such as the application programming interface and/or design of experiment and response surface function of commercial software may be used to determine the highs and lows and the sensitivities of the stresses to a range of bone and implant parameters during implantation. Parameters that can be considered include element deactivation, contact friction, optimum combination of insertion torque/speed, implant diameter, length, tapers, thread design and primary cutting face and secondary cutting flute dimensions for each bone type.

References

1. Irish JD (2004) A 5,500 year old artificial human tooth from Egypt: a historical note. Int J Oral Maxillofac Implants 19(5):645–647
2. Brånemark PI (1983) Osseointegration and its experimental background. J Prosthet Dent 50(3):399–410
3. Bragger U, Krenander P, Lang NP (2005) Economic aspects of single-tooth replacement. Clin Oral Implants Res 16(3):335–341
4. van der Wijk P, Bouma J, van Oort RP, van Waas MA, van't Hof MA, Rutten FF (1996) Cost-effectiveness analysis of dental implants. Ned Tijdschr Tandheelkd 103(10):382–385
5. Albrektsson T, Dahl E, Enbom L, Engevall S, Engquist B, Eriksson AR, Feldmann G, Freiberg N, Glantz PO, Kjellman O (1988) Osseointegrated oral implants. A Swedish multicenter study of 8139 consecutively inserted Nobelpharma implants. J Periodontol 59(5): 287–296
6. Arvidson K, Bystedt H, Frykholm A, von Konow L, Lothigius E (1992) A 3-year clinical study of Astra dental implants in the treatment of edentulous mandibles. Int J Oral Maxillofac Implants 7:321–329

7. Spiekermann H, Jansen VK, Richter EJ (1995) A 10-year follow-up study of IMZ and TPS implants in the edentulous mandible using bar-retained overdentures. Int J Oral Maxillofac Implants 10:231–243
8. Mericski-Stern R, Schaffner TS, Marti P, Geering AH (1994) Peri-implant mucosal aspects of ITI implants supporting overdentures: a five-year longitudinal study. Clin Oral Implants Res 5:9–18
9. Fritz ME (1996) Implant therapy. II. Ann Periodontol 1:796–815
10. Jemt T, Johansson J (2006) Implant treatment in the edentulous maxillae: a 15-year follow-up study on 76 consecutive patients provided with fixed prostheses. Clin Implant Dent Relat Res 8(2):61–69
11. Nobel Biocare (2012) http://www.nobelbiocare.com/. Accessed 12 July 2012
12. Neoss, Pty Ltd (2009) Neoss implant system surgical guidelines. Neoss, Pty Ltd, Harrogate
13. O'Brien WJ (1989) Dent mats: properties and selection. Quintessence Publishing, Chicago/London
14. McClarance E (2004) Close to the cutting edge. Brånemark and the development of Osseointergration. Quintessence Publishing, London
15. Porter JA, von Fraunhofer JA (2005) Success or failure of dental implants? A literature review with treatment considerations. Gen Dent 53(6):423–432
16. Sennerby L, Meredith N (2008) Implant stability measurements using resonance frequency analysis: biological and biomechanical aspects and clinical implications. Periodontol 47(1): 51–66. doi:10.1111/j.1600-0757.2008.00267.x
17. 3i (2013) 3i implant innovations Inc. http://biomet3i.com/. Accessed 13 Apr 2013
18. Lambert FE, Weber HP, Susarla SM, Belser UC, Gallucci GO (2009) Descriptive analysis of implant and prosthodontic survival rates with fixed implant-supported rehabilitations in the edentulous maxilla. J Periodontol 80(8):1220–1230. doi:10.1902/jop.2009.090109
19. Mullender M, EI Haj AJ, Yang Y, van Duin MA, Burger EH, Klein-Nulend J (2004) Mechanotransduction of bone cells in vitro: mechanobiology of bone tissue. Med Biol Eng Comput 42:14–21
20. Miyata T, Kobayashi Y, Araki H, Ohto T, Shin K (2002) The influence of controlled occlusal overload on peri-implant tissue. Part 4: a histologic study in monkeys. Int J Oral Maxillofac Implants 17(3):384–390
21. Tada S, Stegaroiu R, Kitamura E, Miyakawa O, Kusakari H (2003) Influence of implant design and bone quality on stress/strain distribution in bone around implants: a 3-dimensional finite element analysis. Int J Oral Maxillofac Implants 18(3):357–368
22. Petrie CS, Williams JL (2005) Comparative evaluation of implant designs: influence of diameter, length, and taper on strains in the alveolar crest. A three-dimensional finite-element analysis. Clin Oral Implants Res 16(4):486–494
23. Kitagawa T, Tanimoto Y, Nemoto K, Aida M (2005) Influence of cortical bone quality on stress distribution in bone around dental implant. Dent Mater J 24(2):219–224
24. Satoh T, Maeda Y, Komiyama Y (2005) Biomechanical rationale for intentionally inclined implants in the posterior mandible using 3D finite element analysis. Int J Oral Maxillofac Implants 20(4):533–539
25. Perez del Palomar A, Arruga A, Cegonino J, Doblare M (2005) A finite element comparison between the mechanical behaviour of rigid and resilient oral implants with respect to immediate loading. Comput Meth Biomech Biomed Eng 8(1):45–57
26. Sevimay M, Turhan F, Kiliçarslan MA, Eskitascioglu G (2005) Three-dimensional finite element analysis of the effect of different bone quality on stress distribution in an implant-supported crown. J Prosthet Dent 93(3):227–234
27. van Staden R, Guan H, Johnson NW, Loo YC, Meredith N (2008) Step-wise analysis of dental implant insertion process using finite element technique. Clin Oral Implants Res 19(3): 303–313
28. ABAQUS (2013) http://www.simulia.com. Accessed 5 Feb 2013

29. Burstein AH, Reilly DT, Martens M (1976) Aging of bone tissue: mechanical properties. J Bone Joint Surg Am 58(1):82–86
30. Choubey A, Basu B, Balasubramaniam R (2004) Tribological behaviour of Ti-based alloys in simulated body fluid solution at fretting contacts. Mater Sci Eng A 379(1–2):234–239. doi: http://dx.doi.org/10.1016/j.msea.2004.02.027
31. van Staden R (2008) Finite element analysis of dental implant-bone system during and after implantation, PhD thesis. Griffith University, Australia
32. Rieger MR, Mayberry M, Brose MO (1990) Finite element analysis of six endosseous implants. J Prosthet Dent 63(6):671–676
33. O'Mahony A, Bowles Q, Woolsey G, Robinson SJ, Spencer P (2000) Stress distribution in the single-unit osseointegrated dental implant: finite element analyses of axial and off-axial loading. Implant Dent 9(3):207–218
34. Rho JY, Ashman RB, Turner CH (1993) Young's modulus of trabecular and cortical bone material: ultrasonic and microtensile measurements. J Biomech 26(2):111–119